

Spatial coherence considerations for the phase center approximation

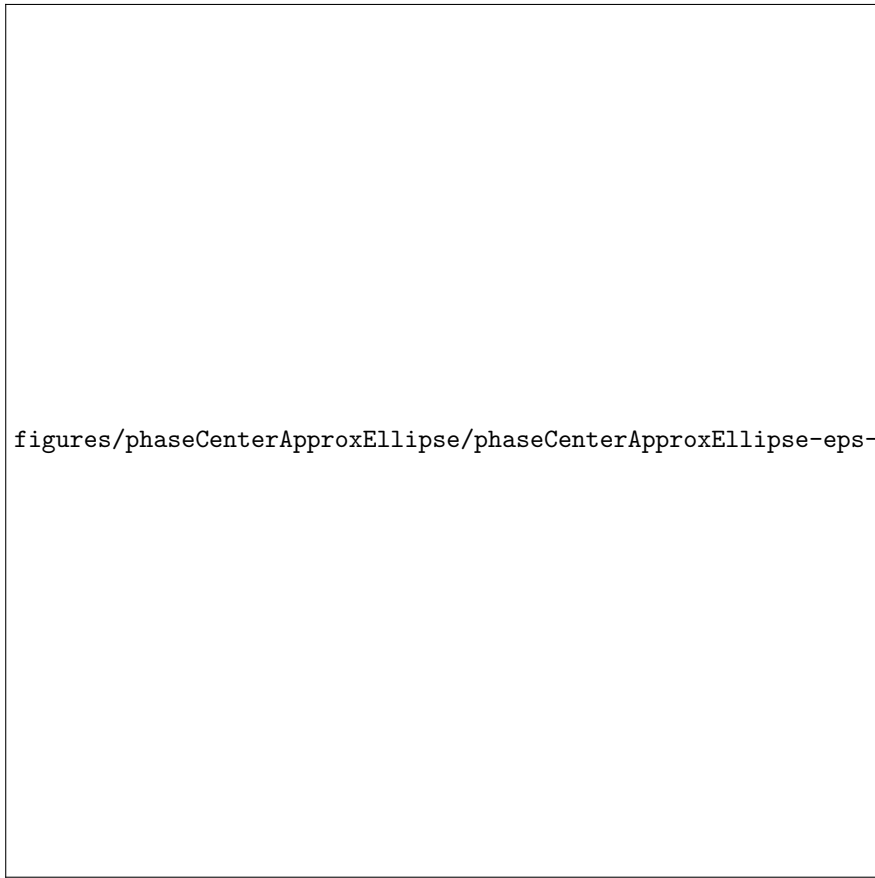
Daniel C. Brown¹ and Thomas Blanford¹

¹Penn State University

January 2, 2023

Abstract

Synthetic aperture sonar image reconstruction relies on the coherence of overlapping phase centers to provide accurate micronavigation for a sensed scene. It is shown that phase centers lose coherence for near-range scattering from large SAS arrays due to the fundamentally bistatic nature of these sensors. This effect is modeled using the van Cittert-Zernike theorem and a point-based sonar scattering model. Reduction of the window length used in the delay estimation process can partially mitigate the loss of coherence at the expense of increased variance in the resulting delay estimates.



figures/phaseCenterApproxEllipse/phaseCenterApproxEllipse-eps-converted-to.pdf

figures/rhoVsRange-PoSSM-vCZT-64/rhoVsRange-PoSSM-vCZT-64-eps-converted-to.pdf

figures/rhoVsRange-PoSSM-vCZT-128/rhoVsRange-PoSSM-vCZT-128-eps-converted-to.pdf

figures/thresholdRange/thresholdRange-eps-converted-to.pdf

figures/vcztGeometryBistatic/vcztGeometryBistatic-eps-converted-to.pdf

Spatial coherence considerations for the phase center approximation

Daniel C. Brown^{1,2} and Thomas E. Blanford¹

¹Applied Research Laboratory - Pennsylvania State University, University Park, PA, USA

²Graduate Program in Acoustics - Pennsylvania State University, University Park, PA, USA

Email: dcb19@psu.edu

Synthetic aperture sonar image reconstruction relies on the coherence of overlapping phase centers to provide accurate micronavigation for a sensed scene. It is shown that phase centers lose coherence for near-range scattering from large SAS arrays due to the fundamentally bistatic nature of these sensors. This effect is modeled using the van Cittert-Zernike theorem and a point-based sonar scattering model. Reduction of the window length used in the delay estimation process can partially mitigate the loss of coherence at the expense of increased variance in the resulting delay estimates.

Background: Synthetic aperture sonar (SAS) sensors create high-resolution imagery of the seafloor through the coherent combination of transmissions from a moving array [1, 2]. Displaced phase center micronavigation is a key technique that permits robust image formation from mobile platforms (e.g. tow sleds or unmanned underwater vehicles) [3, 4]. Many studies and algorithms have been designed leveraging this technique for SAS motion estimation [5–11]. The displaced phase center technique relies on comparisons between pairs of time series recorded on successive pings of a SAS. Under the phase center approximation, signals are fully coherent when their phase centers are co-located. Signals with non-overlapping phase centers may be partially coherent due to the spatial coherence of seafloor scattering. Fundamentally, the displaced phase center method searches for the temporal and spatial offsets maximizing the coherence between signal pairs. These offset estimates are then used to determine the synthetic aperture geometry created by the sensing system.

The phase center approximation assumes the sensed scene is in the far field of the Vernier array formed by the projector and multiple receivers. Many early research SAS sensors deployed small receive arrays [12–14], and the phase center approximation holds across the entire imaging swath for these sensors. More recently developed commercial systems are deploying large receive arrays, and in some cases, these arrays are up to three meters in length [15]. The large separation between the projector and the distal hydrophone on these arrays challenges the validity of the phase center approximation.

This paper focuses on studying the impact of the breakdown of the phase center approximation for a near-range scattered signal for SAS sensors with receive arrays spanning a variety of lengths. First, the phase center approximation itself is reviewed. A model based on the van Cittert-Zernike theorem (vCZT) is utilized to predict the population spatial coherence between signal pairs recorded on successive pings of a bistatic sensor. The predicted population coherence is then compared to a numerical estimate generated through the analysis of an ensemble of pings generated from a point-based scattering model.

Phase Center Approximation: To review the phase center approximation, begin by considering a sonar system consisting of a single transmitter, TX , and receiver, RX . At some instant in time, sensed field is given by the coherent integration of returns from the scatterers located on an isochronous ellipsoid of revolution. Figure 1 shows the ellipse formed by the intersection of the ellipsoid and the x - y plane. The ellipse's foci are located at the transmitter and receiver positions. Except for reciprocal arrangements, unique transmitter and receiver positions produce unique ellipsoids and, therefore, unique sensed fields.

An approximation to the ellipsoidal form can be made for the case where the distance to the ellipsoid's surface is much greater than the transmitter and receiver separation. Assuming that the transmitter and receiver lie along the x -axis, that they are separated by $2d$, and the origin is the midpoint of the line joining the transmitter and receiver, the

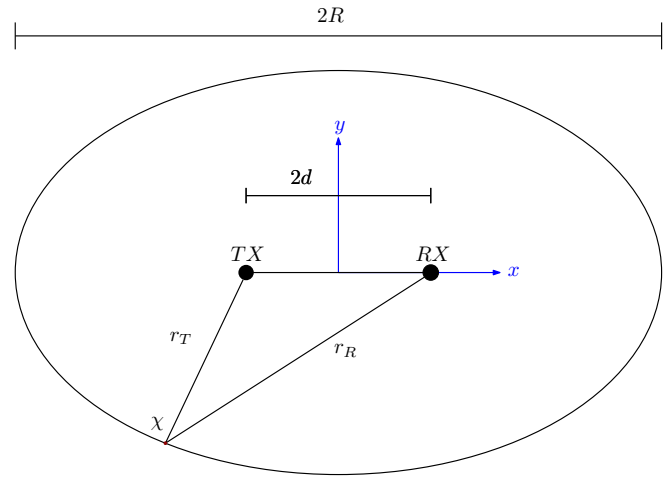


Fig 1 For a bistatic transmitter (TX) and receiver (RX), the field received at some instant in time is due to scattering from an isochronous ellipsoid of revolution. The intersection of this ellipsoid and the x - y plane is shown as an ellipse. For $R \gg d$ this ellipsoid is well approximated as a sphere of radius R centered on the midpoint of TX - RX . This midpoint is known as the phase center.

ellipsoid of revolution is given by

$$\frac{x^2}{R^2} + \frac{y^2}{R^2 - d^2} + \frac{z^2}{R^2} = 1 \quad (1)$$

$$x^2 + \frac{y^2}{1 - \frac{d^2}{R^2}} + z^2 = R^2. \quad (2)$$

In the far field, $R \gg d$ and the ellipsoid is well approximated as a sphere of radius R . Under this approximation, the scattered returns of any bistatic sensor pair can be approximated by a monostatic sensor located at the midpoint between the transmitter and receiver. This midpoint is known as the phase center. The sensed field is due to the integration of scatterers distributed over this spherical surface, and any pair of transmitters and receivers with a common phase center will produce an identical signal. For this reason, the phase center approximation is also described as the “principle of waveform invariance” [16, 17].

The phase center approximation is valid in the far field of the Vernier array when R is larger than the Fraunhofer distance $R \gg 2d^2/\lambda$, where λ is the wavelength [5]. As the range decreases and begins to approach the Fraunhofer distance, the effect of the approximation's breakdown is the introduction of a delay between the signal observed from the monostatic phase center and the signal observed from the bistatic sensor. Correction of this delay is required to achieve high-resolution imagery for most (if not all) practical SAS sensors [18]. When R is much less than the Fraunhofer distance, the monostatic and bistatic signals begin to lose coherence with each other. This effect is similar to the baseline decorrelation of interferometric sonars and radars [19].

Analytic Model for Ping-to-Ping Coherence: The van Cittert-Zernike theorem was developed in the field of statistical optics, and it relates the spatial distribution of the intensity of an incoherent radiator to the coherence of the radiated field measured between two points [20]. This theorem has been adapted to address the spatial coherence of scattered acoustic fields [21, 22]. It has recently been extended to consider the impact of temporal windowing for seabed scattering of pulsed active sonar systems [23]. vCZT-based models for the spatial coherence of the scattered field have motivated the development of algorithms for SAS along-track motion estimation [24, 25].

The vCZT model provided by Brown, Gerg, and Blanford expresses the covariance of a pair of receivers observing temporally-windowed returns of the scattered field generated from a single transmission [24]. This single ping model is applicable to the multi-ping along-track estimation problem when the phase center approximation is valid. To directly evaluate the impact of the bistatic geometry for large synthetic aperture sonar arrays requires explicit consideration of the transmitter and receiver positions on a pair of successive pings.

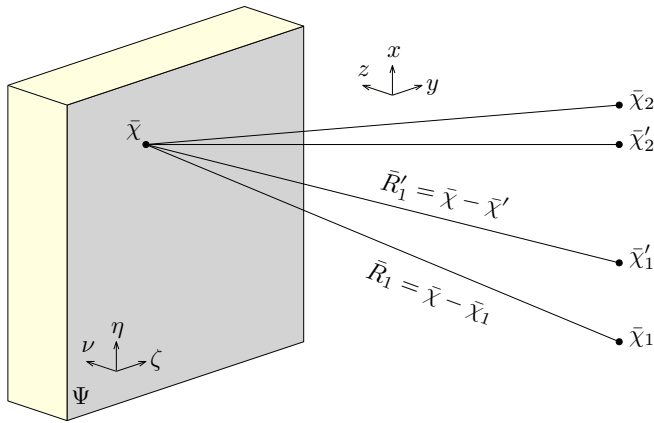


Fig 2 The vCZT is applied in Equation 3 using a geometry where a bistatic sonar transmits a pair of pings from $\bar{\chi}'_1$ and $\bar{\chi}'_2$. After scattering from the surface Ψ , the field is received at $\bar{\chi}_1$ and $\bar{\chi}_2$.

The vCZT model can be directly expanded to consider sequential pings of a bistatic sonar. The covariance, less constant scaling factors, of the field measured on the temporal interval $[t_1, t_2]$ is

$$\gamma_{12}(t_1, t_2) \propto \int_{\Psi} \frac{b'_1(\bar{\chi})b_1(\bar{\chi})}{R'_1 R_1} \Lambda_1(\bar{\chi}, \frac{t_2 + t_1}{2}, t_2 - t_1) \frac{b'_2(\bar{\chi})b_2(\bar{\chi})}{R'_2 R_2} \Lambda_2(\bar{\chi}, \frac{t_2 + t_1}{2}, t_2 - t_1) \sigma(\bar{\chi}) e^{ik(R'_1 + R_1 - R'_2 - R_2)} d\bar{\chi}. \quad (3)$$

The geometry for this equation is provided in Figure 2. The sonar transmits at the positions $\bar{\chi}'_1$ and $\bar{\chi}'_2$ and receives the scattered field at $\bar{\chi}_1$ and $\bar{\chi}_2$, where numeric subscripts indicate ping number. For a high-frequency SAS system, the scattered signal is dominated by the scattering from the surface Ψ . The transmit and receive directivity functions are b' and b respectively. $\sigma(\bar{\chi})$ is the interface scattering strength, and k is the acoustic wavenumber. The temporal interval $[t_1, t_2]$ creates a spatial "masking" of the seafloor, so only a finite region contributes to the field observed at any instant in time. This effect is captured in the masking function, Λ_m , which is defined for ping $m \in [1, 2]$ as

$$\Lambda_m(\bar{\chi}, t, \tau) = \begin{cases} 0 & \text{if } \frac{1}{\tau} |t - \frac{1}{c} |\bar{\chi} - \bar{\chi}_m| - \frac{1}{c} |\bar{\chi} - \bar{\chi}'_m| > \frac{1}{2} \\ \frac{1}{2} & \text{if } \frac{1}{\tau} |t - \frac{1}{c} |\bar{\chi} - \bar{\chi}_m| - \frac{1}{c} |\bar{\chi} - \bar{\chi}'_m| = \frac{1}{2} \\ 1 & \text{if } \frac{1}{\tau} |t - \frac{1}{c} |\bar{\chi} - \bar{\chi}_m| - \frac{1}{c} |\bar{\chi} - \bar{\chi}'_m| < \frac{1}{2}, \end{cases} \quad (4)$$

where c is the sound speed, and τ is the pulse length. Finally, many of the terms in the integrand are shown as dependent on $\bar{\chi}$ to emphasize their role in determining the spatial distribution of intensity creating the scattered field. By using this expression for the covariance of the field, the correlation coefficient can be calculated as

$$\rho_{12}(t_1, t_2) = \frac{\gamma_{12}(t_1, t_2)}{\sqrt{\gamma_{11}(t_1, t_2)\gamma_{22}(t_1, t_2)}}. \quad (5)$$

Signal coherence is commonly expressed using a correlation coefficient. Evaluation of Equations 3 and 5 gives the population correlation of the scattered field for a given sensor, geometry, and environment. For realistic sensors and environments, the integral in Equation 3 is evaluated numerically with a model for the seafloor scattering strength and measurements of the sensor directivity functions.

Simulation and Analysis of Ping-to-Ping Coherence: The vCZT model developed above predicts the population coherence of signals received in sequential pings of a SAS system. In this section, the time series measured by a sensor is directly simulated using a point-based sonar scattering model (PoSSM) [26]. The simulated sensor operates with a center frequency of 200 kHz and a bandwidth of 30 kHz at an altitude of 15 m. The transmitters and receivers are modeled with omnidirectional vertical beam patterns and sinc patterns corresponding to transmit and receive element widths of 4 cm. The SAS is simulated with a single channel of

overlap from ping to ping, and the transmitter and leading receiver channel are assumed to be co-located. Receive array lengths of 0.2 m, 1.2 m, 1.8 m, 2.4 m, and 3.0 m are simulated. The phase center coherence is estimated by the peak magnitude of the complex correlation coefficient calculated from pairs of sliding-window short-time Fourier transforms (STFT). The STFTs are calculated with either 64-point or 128-point windows using rectangular weighting. Sequential short-time windows have 50% overlap.

The vCZT-based population correlation coefficient predicted by Equation 5 is compared to the mean sample correlation coefficient magnitudes calculated from the PoSSM simulations in Figure 3. The correlation coefficient was estimated using the two STFT lengths shown in Figure 3a and 3b, respectively. The model-model agreement is good over most of the simulated sensor ranges. This demonstrates that a long-range SAS sensor's loss of coherence observed at near operating ranges is well captured using a vCZT model. Also, this pair of figures shows that the near-range coherence can be partially recovered by reducing the window length used in the coherence estimation process. There is a disagreement between the models for weakly correlated signals at near ranges. The PoSSM-based simulations exhibit window length dependent asymptotic behavior between 0.2 and 0.3, while the vCZT models predict correlation coefficients that extend to zero.

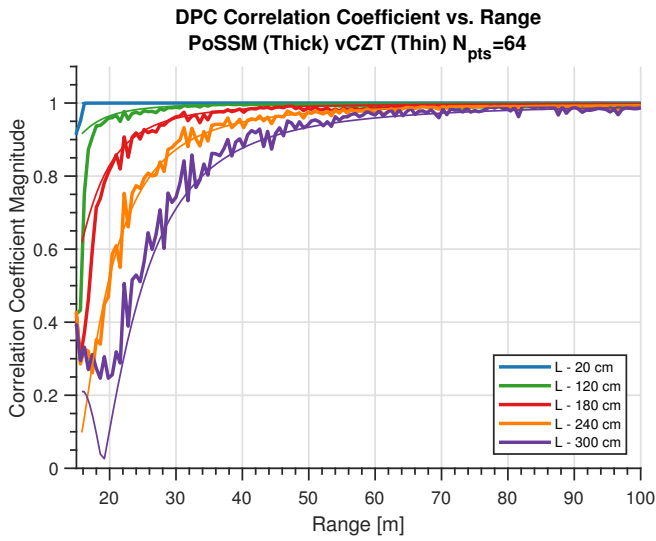
The vCZT-based approach provides a model predicting the true population coherence, while the PoSSM-based approach estimates the coherence from the simulated time series. Therefore, the PoSSM-based approach is subject to the bias error associated with estimation of the magnitude of the complex correlation coefficient. The bias associated with the estimation of the magnitude of the complex correlation coefficient has been widely discussed [27–29]. This bias is further exacerbated by the fact that the coherence estimates are found by calculating the correlation coefficient across a set of temporal lags.

For large receive array lengths, the population coherence does not monotonically increase with increasing range. Instead, $|\rho|$ oscillates between approximately 0 and 0.2. This effect is observed in Figure 3a for the 300 cm array and in Figure 3b for the 240 cm and 300 cm arrays. This ripple phenomenon is a function of both the bistatic separation and the number of points in the STFT window. The complex covariance of the scattered field (mutual intensity in the statistical optics literature) originates at the ensonified region of the seafloor. It propagates to the sensor according to a pair of second-order differential equations [30]. Mathematically, this is similar to the propagation of acoustic pressure via the linearized wave equation. Given the mathematical similarity in their wave equations, there is a close analogy between the spatial coherence in this example and the acoustic pressure radiated from a piston transducer. In the far field of the piston, the acoustic pressure changes slowly with position relative to the source. In the near field, however, the acoustic field has a fine structure with peaks and nulls dependent upon position. The bistatic spatial coherence behaves similarly: the population coherence is very sensitive to position at near range and insensitive to position at far ranges.

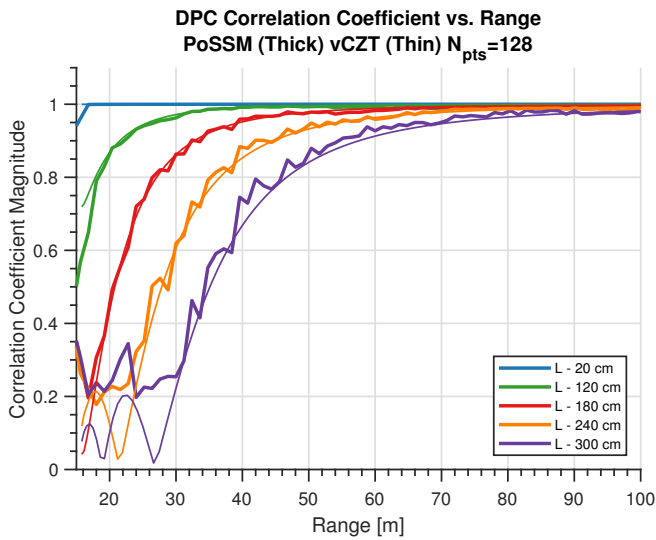
This sensitivity is tied to the complex exponential in Eq. 3. The range of phase angles in the complex exponential term in the integrand is small when the bistatic separation is small compared to the range. At nearer ranges, this term spans a much wider range of angles and the complex exponential term oscillates over the integral. These oscillations cause the value of the integral to be very sensitive to positions.

This near-range ripple effect, however, may be difficult to observe in experimental data. Statistical estimation error introduces bias and variance to the magnitude of complex correlation coefficient, both of which increase with decreasing population coherence [29]. This effect of estimation bias has been observed in SAS systems for speckle coherence [31] and for DPC micronavigation [25]. The challenges with observing this ripple effect are apparent in the PoSSM simulated time-series data. Statistical estimation error causes the correlation coefficient magnitude estimates to plateau at short range to values greater than the ripple amplitude. The increased variance in these estimates (compared to the regions of higher coherence in the plot) further obscures the ripples.

Nonetheless, figure 3 exhibits a trend that is an important consideration for motion estimation design: at near ranges, there is a loss of coherence that depends both on the window length and the bistatic separation. Figure 4 shows the slant range at which the population coherence



(a)



(b)

Fig 3 The population coherence predicted by the vCZT model is compared to the mean sample coherence estimated from PoSSM simulated time-series using STFT windows of (a) 64 points and (b) 128 points. Mismatch for low coherence values is due to bias in estimation of the magnitude of the complex correlation coefficient from the time-series data.

of overlapping phase centers exceeds 0.99 ($|\rho_{12}| > 0.99$) as a function of the bistatic separation length for several STFT window lengths. At this value of population coherence, the breakdown of the phase center approximation has essentially no effect on motion estimation. This loss of coherence is the same as would be experienced for perfectly coherent signals with 20 dB signal-to-noise ratio (SNR) above additive incoherent noise. As the bistatic separation increases, it is necessary to compare signals from further out in range to ensure they will be coherent. This minimum range, however, also increases for longer STFT windows.

As the range increases, the bistatic separation gradually becomes small compared to the distance to the ensonified region of the seafloor. This trend of the bistatic separation becoming small compared to the range eventually results in the validity of the phase center approximation. This relationship explains some of the recovery in coherence. Note, however, that the Fraunhofer distance at the center frequency for the 300 cm array is 2.4 km, assuming $c = 1500 \text{ m s}^{-1}$. The $|\rho_{12}| > 0.99$ threshold occurs at ranges much shorter than the Fraunhofer distance for all of the bistatic separations considered here. The STFT window length is proportional to the size of the ensonified region of the seafloor, and this dimension also is a factor. (When the range exceeds the Fraunhofer distance for the array, the coherence is no longer dependent on the size of

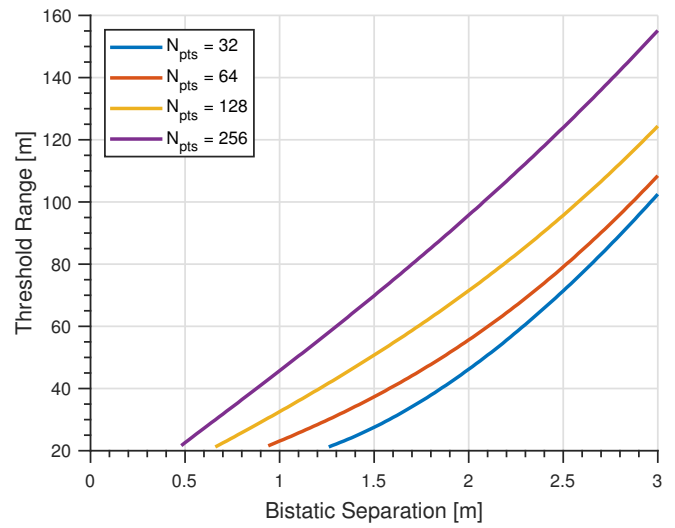


Fig 4 Loss of coherence is observed at near operating ranges for increasing bistatic separation. The slant range at which the population coherence degrades to $\rho_{12} = 0.99$ is plotted as a function of the bistatic separation for STFT windows of 32, 64, 128, and 256 points. As the bistatic separation increases it becomes necessary to use shorter STFT windows in the time delay estimation process used in DPC motion estimation algorithms.

the ensonified patch of seafloor.) At long ranges, however, SNR may be less than 20 dB and cause the coherence to degrade below this threshold. Lower thresholds may be appropriate for very long-range sensors.

These effects have implications for designing long range SAS arrays and motion estimation algorithms. Using short windows can recover some coherence loss, but it comes at the expense of increased statistical estimation error in the magnitude of the complex sample correlation coefficients and the estimation error of the associated time delays. The variance in the correlation coefficient estimates is inversely proportional to the length of the window used in the estimate. For the time delays, the variance in the estimates is inversely proportional to the square root of the length of the window. Greater variance in the sample correlation coefficient magnitudes and the estimated time delays will lead to greater ping-to-ping errors in the sensor's along-track and cross-track motion estimates, respectively.

Conclusion: This paper has investigated the breakdown of the phase center approximation for near-range scattering observed by SAS sensors. This was accomplished through modeling with the vCZT to predict the population coherence and PoSSM to generate an ensemble of pings from which the sample coherence can be estimated. The vCZT method was extended to address fully bistatic scattering from sequential pings of a SAS. The vCZT and PoSSM models agree well, showing that near-range coherence is impacted by the bistatic collection geometry of large arrays. With increasing bistatic separation, a ripple effect is observed in the population coherence at near range; however, this phenomenon was found to be challenging to observe in data as it is obscured by statistical estimation error. The bistatic coherence was found to depend on the window length used to estimate the correlation coefficient, which provides a method to mitigate coherence loss at near ranges. These effects, however, may have important implications for the design of long-range SAS arrays and motion estimation algorithms. Most long-range SAS surveys will operate at altitudes that mitigate these issues. For short-range imaging with a long-range sensor, the degradation of coherence by the breakdown of the phase center approximation and additive noise, when compounded by statistical estimation error, may place practical limits on how the SAS sensor is employed and the design of the associated motion estimation algorithms.

Acknowledgments: This work was supported by the Office of Naval Research under grant N00014-18-1-2820.

© 2022 The Authors. *Electronics Letters* published by John Wiley &

Sons Ltd on behalf of The Institution of Engineering and Technology
This is an open access article under the terms of the Creative Commons Attribution License, which permits use, distribution and reproduction in any medium, provided the original work is properly cited.
Received: 10 January 2021 Accepted: 4 March 2021
doi: 10.1049/ell2.10001

References

- Hayes, M.P., Gough, P.T.: Synthetic aperture sonar: A review of current status. *IEEE J. Oceanic Eng.* 34(3), 207–224 (2009). doi:10.1109/JOE.2009.2020853
- Hansen, R.E.: Introduction to synthetic aperture sonar. InTechOpen (2011)
- Raven, R.S., inventor; Westinghouse Electric Corporation, assignee. Electronic stabilization for displaced phase center systems. 4244036 (1981)
- Sheriff, R.W.: Synthetic aperture beamforming with automatic phase compensation for high-frequency sonar. In: *IEEE Proc. 1992 Symposium on Autonomous Underwater Vehicle Techn.*, pp. 236–245. Washington, DC (1992)
- Belletini, A., Pinto, M.A.: Theoretical accuracy of synthetic aperture sonar micronavigation using a displaced phase centre antenna. *IEEE J. Oceanic Eng.* 27(4), 780–789 (2002)
- Cook, D.A., et al.: Results from a hybrid synthetic aperture sonar motion estimation scheme. In: *MTS/IEEE OCEANS Conf.*, vol. 2, pp. 1376–1381. Brest, France (2005)
- Oeschger, J.W.: Estimating along-track displacement using redundant phase centers. In: *Proceedings of the Institute of Acoustics*, vol. 28, pp. 160–167. (2006)
- Groen, J.: Adaptive Motion Compensation in Sonar Array Processing. Delft University of Technology (2006)
- Cook, D.A., Brown, D.C., Fernandez, J.E.: Synthetic aperture sonar motion estimation using nonlinear least squares. In: *Proc. Institute of Acoustics*, vol. 28, pp. 176–182. (2006)
- Cook, D.A.: Synthetic Aperture Sonar Motion Estimation and Compensation. Georgia Institute of Technology (2007)
- Hunter, A.J., Dugelay, S., Fox, W.L.J.: Repeat-pass synthetic aperture sonar micronavigation using redundant phase center arrays. *IEEE J. Oceanic Eng.* 41(4), 820–830 (2016). doi:10.1109/JOE.2016.2524498
- Fernandez, J.E., et al.: Synthetic aperture sonar development for autonomous underwater vehicles. In: *MTS/IEEE OCEANS Conf.*, vol. 4, pp. 1927–1933. Kobe, Japan (2004)
- Matthews, A.D., et al.: 12.75" synthetic aperture sonar SAS, high resolution and automatic target recognition. In: *MTS/IEEE OCEANS Conf.*, pp. 1–7. Boston, MA (2006)
- Brown, D.C., Cook, D.A., Fernandez, J.E.: Results from a small synthetic aperture sonar. In: *MTS/IEEE OCEANS Conf.*, pp. 1–6. Boston, MA (2006)
- iXblue Inc.: Sams-50 datasheet. <https://www.ixblue.com/wp-content/uploads/2021/12/sams-50-deep-tow.pdf> (2022)
- Dickey, F.R., Edward, J.A.: Velocity measurement using correlation sonar. In: *Proceedings IEEE Position Location and Navigation Symposium*, pp. 255–264. San Diego, CA (1978)
- Bradley, S.E., Deines, K.L., Rowe, F.D.: Acoustic correlation current profiler. *IEEE J. Oceanic Eng.* 16(4), 408–414 (1991). doi:10.1109/48.90906
- Bonifant, W.W.: Interferometric synthetic aperture sonar processing. Georgia Institute of Technology (1999)
- Zebker, H.A., Villasenor, J.: Decorrelation in interferometric radar echoes. *IEEE Trans. Geosci. Remote Sensing* 30(5), 950–959 (1992)
- Born, M., Wolf, E.: *Principles of Optics*. 7th ed. New York: Cambridge University Press (1999)
- Mallart, R., Fink, M.: The van Cittert-Zernike theorem in pulse echo measurements. *J. Acoust. Soc. Am.* 90(5), 2718–2727 (1991). doi:10.1121/1.401867
- Dahl, P.H.: Observations and modeling of angular compression and vertical spatial coherence in sea surface forward scattering. *J. Acoust. Soc. Am.* 127(1), 96–103 (2010). doi:10.1121/1.3268594
- Brown, D.C.: Modeling and Measurement of Spatial Coherence for Normal Incidence Seafloor Scattering. The Pennsylvania State University (2017). <http://etda.libraries.psu.edu/catalog/13741dcb19>
- Brown, D.C., Gerg, I.D., Blanford, T.E.: Interpolation kernels for synthetic aperture sonar along-track motion estimation. *IEEE J. Oceanic Eng.* 45(4), 1497–1505 (2020). doi:10.1109/JOE.2019.2921510
- Thomas, B., Hunter, A.: Coherence-induced bias reduction in synthetic aperture sonar along-track micronavigation. *IEEE J. Oceanic Eng.* 47(1), 162–178 (2022). doi:10.1109/JOE.2021.3103264
- Brown, D.C., Johnson, S.F., Olson, D.R.: A point-based scattering model for the incoherent component of the scattered field. *J. Acoust. Soc. Am.* 141(3), EL210–EL215 (2017). doi:10.1121/1.4976584
- Goodman, N.R.: On the joint estimation of the spectra, cospectrum, and quadrature spectrum of a two-dimensional stationary Gaussian process. University Heights, NY: New York University - Engineering Statistics Laboratory (1957). 10
- Carter, G.C., Nuttall, A.H.: Statistics of the estimate of coherence. *Proc. IEEE* 60(4), 465–466 (1972). doi:10.1109/PROC.1972.8671
- Carter, G.C., Knapp, C.H., Nuttall, A.H.: Statistics of the estimate of the magnitude-coherence function. *IEEE Trans. Audio Electroacoust.* 21(4), 388–389 (1973)
- Goodman, J.W.: *Statistical Optics*. New York, NY: John Wiley and Sons (1985)
- Synnes, S.A.V., Hansen, R.E., Sæbø, T.O.: Spatial coherence of speckle for repeat-pass synthetic aperture sonar micronavigation. *IEEE J. Oceanic Eng.* 46(4), 1330–1345 (2021). doi:10.1109/JOE.2021.3060812